# Breakouts: Physical and Numerical Modeling

Flavia M.G. Villarroel, PUC/DEC, Brazil
Vinicios A. de Azevedo, UENF/LENEP, Brazil
Mauro Bloch, PETROBRAS/CENPES, Brazil
Roseane M. Missagia, UENF/LENEP, Brazil
Eurípedes V.A. Júnior, PUC/DEC, Brazil



This paper was prepared for presentation during the 11th International Congress of the Brazilian Geophysical Society held in Salvador, Brazil, August 24-28, 2009.



## Abstract

In-Situ stress knowledge is very important for the oil industry, affecting well location, drilling, stimulation design, and production rates. Breakout detection from the interpretation of wellbore logs, including geophysical measurements, is one of the most applied methods for estimating the horizontal in-situ stresses. This paper presents laboratory tests for breakout simulation with a synthetic sandstone (0.3 X 0.3 X 0.3 m), performed in a large poliaxial cell. The testing apparatus was able to show breakout formation in a central hole in the block, simulating a vertical wellbore. The experimental results were compared to a numerical simulation through finite elements using a commercial software – ANSYS™ ANSYS, 2007), and to analytical calculations. The breakout formation in the experiments was confirmed from the numerical simulations. The stress contrast at the onset of the breakout failure, as determined from the experimental results, agreed within 2.5 % to the value computed from the numerical and analytical analyses.

## Introduction

Estimating the in-situ stress field deep underground has always been a challenge for the oil industry, and several methods are applied with some degree of success (Bloch et al, 2005). Among these, breakout observation can be considered as the most direct one, since it is caused exactly by the in-situ stress contrast at a certain depth.

Breakouts are defined as regions where the cross-section of mainly vertical wellbores become non-circular due to a non-hydrostatic horizontal stress field and low wellbore internal pressure. Very reliable indicator for the stress orientation, breakout amplitudes can also be correlated to the horizontal stress magnitude, providing the complete stress field.

Methods for breakout identification include the conventional four and six arms dipmeter; borehole image logs; micro-resistivity logs; and acoustic imaging tools (Tingay et al, 2008). Breakouts have been observed in North America, Europe and Brazil (Teufel et al, 1984; Dart and Zoback, 1985; Bell, 1990; Fejerskov and Bratli, 1998; Conceição, 1996; Lima and Nascimento, 1994), helping the determination of the in-situ stress field whenever the necessary conditions for breakout assurance are met.

## Breakout Analysis

Breakout failure are caused by shear stresses (Fjaer et al, 2008), exactly at the maximum tangential stress point in the wellbore wall section, which according to the Kirsch solution for circular openings under compression (Goodman, 1989), is perpendicular to the maximum stress ($S_{max}$) orientation, aligned thus to the minimum stress ($S_{min}$), as shown in Figure 1.

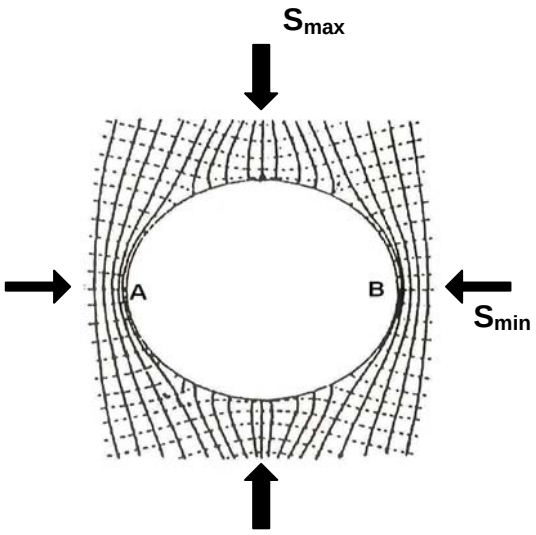


**Figure 1:** Stress lines showing the critical points A and B of a circular opening in a biaxial stress field (Zoback, 2009).

Nevertheless, well engineers must carefully analyze breakout information from caliper logs, in order to be sure that they are really seeing breakouts instead of drill pipe wear, washouts or key seats that can also cause borehole enlargements. The conditions for breakout assurance are (Bloch, 1999; Reinecker et al, 2003):

1. stress contrast high enough for the critical stress to exceed the rock strength;
2. caliper difference has to exceed the drilling bit size by 10%;
3. the enlargement orientation should not coincide with the high side of the borehole, in wells deviated by more than 5 degrees;
4. the length of the enlargement zone must be greater than 1 meter.

### Physical Modeling

Laboratory tests for reproducing breakout with large samples have been made by a few authors (Kooijman, et al, 1992; Van Dam et al, 1999; Haimson, and Lee, 2004; Haimson, 2007;), but can still be considered a non usual study, due to the need of large laboratory equipments.

The present work was conducted in the large poliaxial cell of the Petrobras Research and Development Center – CENPES, in Rio de Janeiro, Brazil (Villarroel, 2009). Cubic rock samples, with a central hole simulating a vertical wellbore, were mechanically compressed in the two perpendicular directions (simulating the maximum and minimum horizontal stress orientation) by 4 pistons, each one with a maximum pressure of 62 MPa manually controlled within ± 0.13 MPa. The pistons could be independently pressurized, allowing the simulation of any horizontal stress state. An overview of the testing frame is shown in Figure 2.

An advantage of this large-scale laboratory test was minimizing border effects, allowing thus a better representation of the analyzed phenomena.

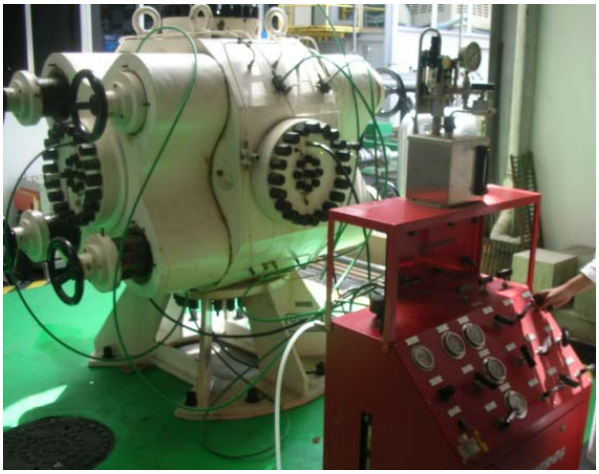

**Figure 2:** Poliaxial cell and controlling valves.

### Sample Preparation

Preparing large, real rock specimens, nevertheless, is not easy. Because of this, the experiments were conducted on artificial rock samples: cubic blocks measuring 0.30 X 0.30 X 0.30 m with a centered hole of 0.06 m diameter were made of cement, sand and water. Each component was carefully measured to achieve the same specific ratio for all the samples. After the curing process a final polishing was conducted providing the better orthogonality possible between the sample sides, avoiding non-representative results.

### Material Characterization

Cylindrical samples, prepared with the same material as the cubic blocks, were used for mechanical properties determination in compression tests. Thin sections for the Scanning Electron Microscope (SEM) and mineralogy analysis were also obtained. Table 1 shows a summary of the material characterization.

**Table 1:** Material Characterization.

| Testing | Results |
|---|---|
| Triaxial compression | Cohesion: 2,77 MPa |
| | Friction angle: $34{,}76^0$ |
| Uniaxial compression | UCS: 9,06 MPa |
| | Young's modulus: 2,4 GPa |
| | Poisson's ratio: 0,3 |
| Mineralogy analysis | Mostly quartz |
| Grain analysis | Fine (poorly sorted) |

### Testing Procedure

Paper-made spacers, greased with vaseline and stearic acid, were used to reduce friction between the block and the loading platens in the cell, and to minimize border effects. Figure 3 shows the block inside the poliaxial frame, before instrumentation.

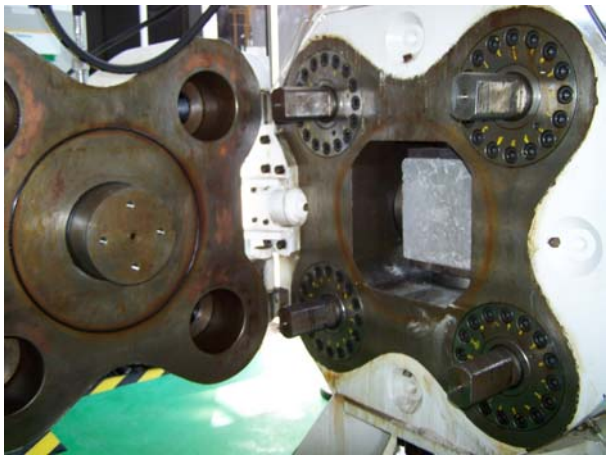

**Figure 3:** Block inside the poliaxial frame.

The cubic block was loaded until the stress level needed for full breakout identification. In the first stage, the sample was loaded and unloaded twice, in both directions, at 1.38 MPa and 2.59 MPa, for checking the system. In the second step, the pressure from the top and bottom actuators (maximum stress orientation perpendicular to the hole axis) was then increased up to 8.63 MPa. This pressurization was kept for 5 more minutes, before depressurizing the system.

### Experimental Results

Three poliaxial tests were performed with the loading previously explained. Table 2 shows the principal stresses ($S_{Hmax}$ and $S_{hmin}$) perpendicular to the hole axis at the breakout onset.

**Table 2:** Experimental results: stresses at the breakout onset (MPa).

| | Sample A | Sample B | Sample C |
|---|---|---|---|
| $S_{Hmax}$ | 5.18 | 5.18 | 6.04 |
| $S_{hmin}$ | 2.59 | 2.59 | 2.59 |
| $S_{Hmax}/ S_{hmin}$ | 2.00 | 2.00 | 2.33 |

Pictures with the breakout initiation (at $S_{Hmax}$ = 5.18 MPa and $S_{hmin}$ = 2.59 MPa) and the final breakout shape ($S_{Hmax}$ = 8.63 MPa and $S_{hmin}$ = 2.59 MPa) are shown in Figure 4.

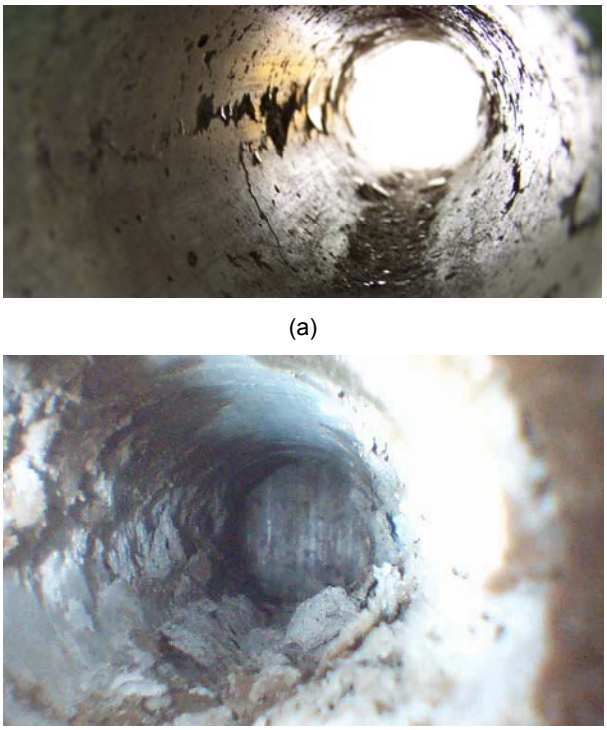

(a)

(b)

**Figure 4:** Breakout at the hole lateral wall, recorded with a webcam at: (a) beginning of the breakout; (b) at the end of a test.

In order to capture the breakout final shape, the hole was filled up with resin at the end of two tests, giving a better idea of the localized collapse (fig. 5).


**Figure 5:** Resin mold showing the inside of the hole after breakout for samples A and B (left and right), and the original hole circular shape (center).

**Numerical Modeling**

A finite element method – FEM (ANSYS$^{TM}$ software – ANSYS, 2007), was used for analyzing the stress and strain distribution in a cubic block with a central hole – identical to the physical model, and the same boundary conditions. A plane strain - linear elastic approach was considered, since this is the most common procedure (Amadei, 1997) for breakout simulations. A quadratic mesh, instead of a free mesh, was chosen within the ANSYS options, due to its recognized higher accuracy.

The steps taken in the numerical modeling can be summarized as:

1. Model Formulation: geometry definition; input of the rock mechanical properties and selection of the boundary conditions; mesh generation;
2. Stress Loading: the pressure applied on the block sides, perpendicular to the hole axis, was 2.59 MPa at the simulation starting point. The pressure on one direction was then increased up to 8.63 MPa, simulating the same stress condition as in the experimental test with samples A and B;
3. Running the program with the convergence criterion of 0.001, selected as the best option regarding computational time and accuracy, after a few trials;
4. Stress and Strains were computed at each 30 seconds during the load application (total loading time of 720 s).

Mesh refinement was also applied for optimizing the final result, as shown in Table 3.

**Table 3:** Mesh refinement for the numerical simulation.

| Run | Mesh size | Running time |
|---|---|---|
| 1 | 0.220 | |
| 2 | 0.200 | 1 hour |
| 3 | 0.180 | |
| 4 | 0.150 | 3 hours |
| 5 | 0.120 | |
| 6 | 0.110 | 18 hours |
| Standard deviation/average value for all the runs at the final step (720 s) | | 2.06% |
| Change in the final value at the final step (720 s) from run 1 to 6 | | 0.50% |

Figure 6 shows the loading path for each mesh size analyzed, at the critical points A and B, with approximately the same pattern as in the experimental work: several steps of loading and holding the load constant. The Kirsch solution was applied, showing a much higher stress level because of the stress concentration at A and B.

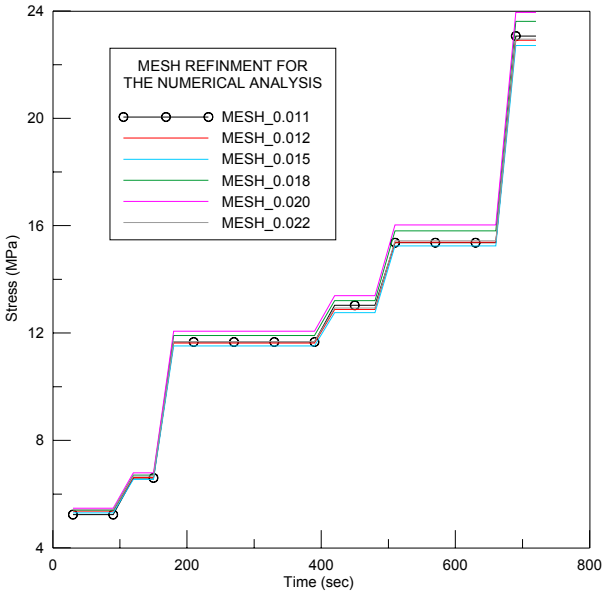


**Figure 6:** Loading path for each utilized mesh, showing the maximum stress at the hole internal wall, exactly at the critical points A and B.

### Numerical Results

The numerical simulations were run with the loading path shown in Figure 6, for a homogeneous and isotropic rock, with the mechanical properties from Table 1.

Figure 7 shows the stresses around the hole and at hole internal wall surface, 120 seconds after loading initiation. At this moment, the stress concentration at the critical points was not enough yet for causing breakouts.

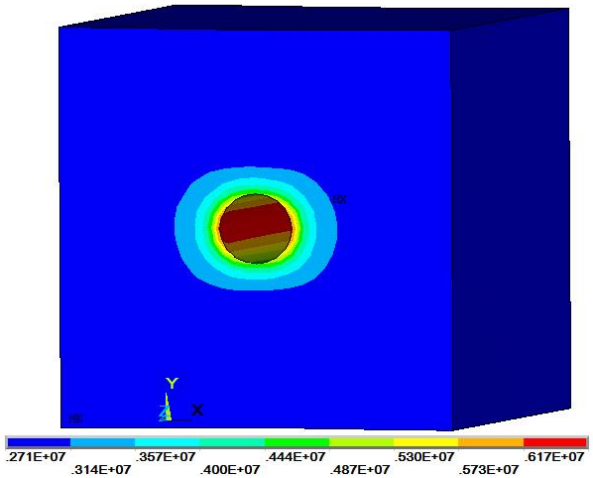


**Figure 7:** Stress Field at t = 120 s, mesh 0.011.

At t = 420 s, breakout was detected in the hole internal wall, with the stress condition shown in Table 4. Figure 8 shows the stress distribution in the block and at the hole internal wall.

**Table 4:** Numerical results: stresses at the breakout onset (MPa).

| Stress | Critical Points | Block wall |
|---|---|---|
| $S_{Hmax}$ | 12.20 | 5.18 |
| $S_{hmin}$ | 6.10 | 2.59 |
| $S_{Hmax}$/ $S_{hmin}$ | 2.00 | 2.00 |

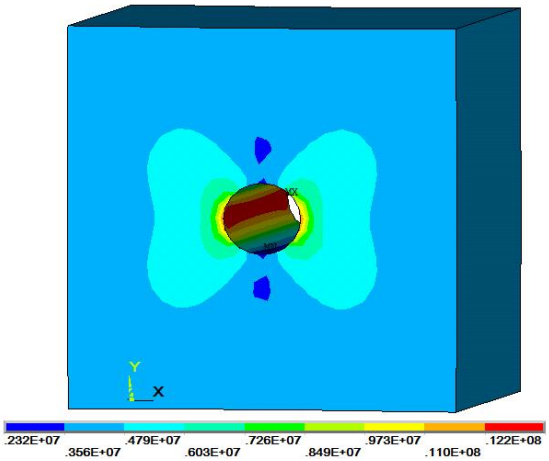


**Figure 8:** Stress Field at t = 420 s, mesh 0.011.

The strain pattern after breakout (t = 420 s) is shown in Figure 9.

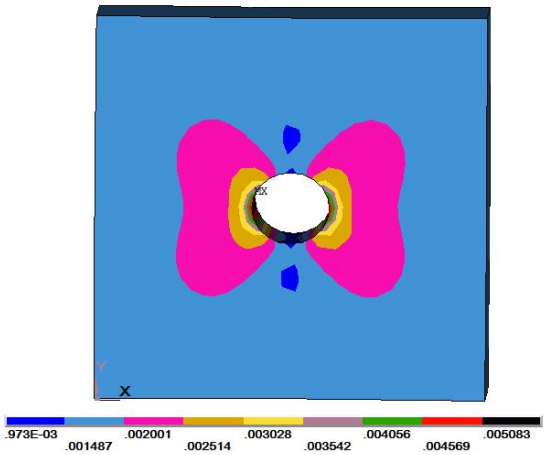


**Figure 9:** Strain distribution at t = 420 s, mesh 0.011.

### In-Situ Stress Magnitude

The theory of breakout states that the horizontal in-situ stress magnitudes can be computed from the hole final enlargement (Amadei et al,1997; Zoback et al, 1985; Zoback, 2007). In order to corroborate the stresses from the experimental work and the numerical approach, the theoretical model was applied considering:

1. The principal stresses are perpendicular to the hole axis, and since the theory has been written

for vertical oil wells, they are named $S_{Hmax}$ and $S_{hmin}$;

2. The rock is homogeneous, isotropic and linear elastic

3. Stresses are constant.

The radial and tangential stress component at any point (r,θ) in a horizontal plane can be given by (Amadei, 1997):

$$\sigma_r = \left(1-\frac{R^2}{r_b^2}\right)\cdot\frac{(S_{H\,max}+S_{h\,min})}{2} + \left(1+3\cdot\frac{R^4}{r_b^4}-4\cdot\frac{R^2}{r_b^2}\right)\cdot\frac{(S_{H\,max}-S_{h\,min})}{2}\cdot cos(2\theta)+\Delta P\cdot\frac{R^2}{r_b^2} \quad (1)$$

$$\sigma_\theta = \left(1+\frac{R^2}{r_b^2}\right)\cdot\frac{(S_{H\,max}+S_{h\,min})}{2} - \left(1+3\cdot\frac{R^4}{r_b^4}\right)\cdot\frac{(S_{H\,max}-S_{h\,min})}{2}\cdot cos(2\theta)-\Delta P\cdot\frac{R^2}{r_b^2} \quad (2)$$

$$\tau_{r\theta} = -\left(1-3\cdot\frac{R^4}{r_b^4}+2\cdot\frac{R^2}{r_b^2}\right)\cdot\frac{(S_{H\,max}-S_{h\,min})}{2}\cdot sin(2\theta) \quad (3)$$

Where:

$\sigma_r$ = radial stress;
$\sigma_\theta$ = tangential stress;
$\tau_{r\theta}$ = shear stress;
$\Delta P$ = assumed to be zero, since there was no fluid in the hole neither in the rock pore spaces.

Assuming the Mohr-Coulomb failure criterion, the failure envelope is such that:

$$|\tau| = C+\mu\sigma \quad (4)$$

Cohesion can be written as a function of stresses by:

$$C = \left(1+\mu^2\right)^{\frac{1}{2}}\cdot\left(\left(\frac{\sigma_\theta-\sigma_r}{2}\right)^2+\tau_{r\theta}^2\right)^{\frac{1}{2}}-\mu\cdot\left(\frac{\sigma_\theta+\sigma_r}{2}\right) \quad (5)$$

With equations 1, 2 and 3 into 5, the horizontal in-situ stress ratio can be written as a function of the rock parameters and the breakout final shape:

$$\frac{S_{H\,max}}{S_{h\,min}} = \frac{(d-b)}{(a-c)} \quad (6)$$

$$S_{H\,max} = 2\cdot C\cdot\frac{(d-b)}{(a\cdot d-b\cdot c)} \quad (7)$$

$$S_{h\,min} = 2\cdot C\cdot\frac{(a-c)}{(a\cdot d-b\cdot c)} \quad (8)$$

Where:

$$a = \left(\left(1+\mu^2\right)^{\frac{1}{2}}-\mu\right)\cdot\left(1-2\cdot cos(2\theta_b)\right) \quad (9)$$

$$b = \left(\left(1+\mu^2\right)^{\frac{1}{2}}-\mu\right)\cdot\left(1+2\cdot cos(2\theta_b)\right) \quad (10)$$

$$c = \left(\left(1+\mu^2\right)^{\frac{1}{2}}-\mu\right) - \frac{R^2}{r_b^2}\cdot\left(\left(1+\mu^2\right)^{\frac{1}{2}}+2\mu\right)+3\cdot\frac{R^4}{r_b^4}\cdot\left(\left(1+\mu^2\right)^{\frac{1}{2}}\right) \quad (11)$$

And the breakout shape is expressed by:

$$\theta_b = 90-\phi_b/2\ , \quad (12)$$

according to the geometry shown in Figure 10.

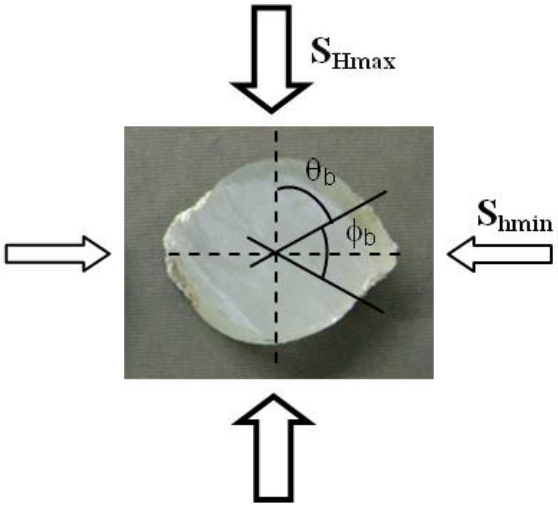


**Figure 10:** Breakout angles for the calculation of the in-situ stress magnitude:

- $\theta_b$ is the angle between $S_{Hmax}$ and the beginning of the collapsed zone;
- $\phi_b$ is the angle indicating the breakout amplitude.

The input parameters and the results for the analytical calculation are shown in Table 5.

**Table 5:** Input parameters for the breakout geometry and in-situ stress ratio calculated from the analytical approach.

| Parameters | Sample A | Sample B |
|---|---|---|
| Friction coefficient (μ) | 0.694 | 0.694 |
| Cohesion (c) | 2.77 MPa | 2.77 MPa |
| Borehole radius (R) | 3.00 cm | 3.00 cm |
| Deformed radius in the Breakout zone ($r_b$) | 1.5978 cm | 1.5897 cm |
| Breakout angle ($\theta_b$) | $52.16^0$ | $53.94^0$ |
| Breakout angle ($\phi_b/2$) | $37.84^0$ | $36.06^0$ |
| $S_{Hmax}/S_{hmin}$ | 2.03 | 2.05 |

## Conclusions

The breakout physical simulation was well succeeded, opening the option for further similar analyses with the poliaxial frame. The experimental results correlated very well to the numerical and analytical solution: the breakout formation seen in the experiments was confirmed by the numerical approach, and the stress magnitude ratio, from the three approaches was within 2.5 %, as shown in Table 6.

**Table 6:** Comparison among the experimental, numerical and analytical results (MPa).

| | Experimental | Numerical | Analytical |
|---|---|---|---|
| $S_{Hmax}$ | 5.18 | 5.18 | - |
| $S_{hmin}$ | 2.59 | 2.59 | - |
| $S_{Hmax}$/ $S_{hmin}$ | 2.00 | 2.00 | 2.03 - 2,05 |

## Acknowledgments

The authors wish to thanks the North State Fluminense University of Rio de Janeiro – UENF, the Catholic University of Rio de Janeiro – PUC-RIO, and the Petrobras Research and Development Center – CENPES, for giving the financial and material support for this work.

## References

**Amadei, B., and Stephansson, O.** 1997, 1st Edition, Rock Stress And Its Measurement, Chapman & Hall, London, England.

**Ansys™** 2007, Release 11.0. Documentation for Ansys.

**Bell, J.S.** 1990, The Stress Regime of Scotian Shelf Offshore Eastern Canada to 6 Kilometers Depth and Implications for Rock Mechanics and Hydrocarbon Migration, Rock at Great Depth, pp 1243-1265, Balkema Ed., Rotterdam, Holland.

**Bloch, M.** 1999, In-Situ Stress in Porous Formation, Ph.D. Thesis, Oklahoma, USA.

**Bloch, M., Freitas, S.M.S., Socorro, M., Soares, J.A., and Bacelar, C.J.R.** 2005, In-Situ Stress Determination Based Upon Borehole Imaging and Rock-Sample Analyses: a Comparison Among Anelastic Strain Recovery (ASR), Acoustic Velocity and Acoustic Tomography, SPE 94919, Rio de Janeiro, Brazil.

**Conceição, J.C.J.** 1996, Análise de Tensões Neotectônicas pelo Método de Breakouts na Área do Campo de Garoupa, Bacia de Campos, Internal Report CENPES/PETROBRAS, Rio de Janeiro, Brazil.

**Dart, R.L., and Zoback, M.L.** 1985, Wellbore Breakout Analyses within the Continental United States, 2nd International Symposium on Borehole Geophysics for Minerals, Geotechnical and Ground Water Applications, pp. 1-11, Soc. of Prof. Well Log Analysts Publ., Golden, USA.

**Fjaer, E., Holt, R.M., Horsrud, P. Raaen, A.M. and Risnes, R.** 2008, Petroleum Related Rock Mechanics, 2nd Edition, Elsevier Science Publishers, Amsterdam, Holland.

**Fjerskov, M., and Bratli, R.** 1998, Can Dipmeter Logs be Used to Indentify In-Situ Stress Direction in the North Sea, SPE/ISRM 47237, Eurock'98, Trondheim, Norway.

**Goodman, R.E.** 1989, Introduction to Rock Mechanics, John Wiley & Sons, New York, USA.

**Haimson, B.C. and Lee, H.** 2004, Borehole breakouts and compaction bands in two high porosity sands. International Journal of Rock Mechanics and Mining Sciences, Vol. 41. pp.287-301.

**Haimson, B.C.** 2007, Micromechanisms of borehole instability leading to breakouts in rocks. International Journal of Rock Mechanics and Mining Sciences, Vol. 44. pp. 157-173.

**Kooijman, A.P., et al.** 1992, Large-scale laboratory sand production test. SPE Annual Technical Conference and Exhibition, Washington DC, USA.

**Lima, C.C., and Nascimento, E.M.** 1994, Determinação das Direções de Tensão Máxima Horizontal ($S_{Hmax}$) nas Bacias Sedimentares Brasileiras Através da Análise de Breakouts, Internal Report CENPES/PETROBRAS, Rio de Janeiro, Brazil.

**Reinecker, J., Tingay, M., and Müller, B.** 2003, Borehole Breakout Analysis from Four-arm Caliper Logs, World Stress Map Project.

**Teufel, L.W., Hart, C.M., and Sattler, A.R.** 1984, Determination of Hydraulic Fracture Azimuth by Geophysical, Geological, and Oriented Core Methods at the Multiwell Experiment Site, SPE 13226, Rifle, USA.

**Tingay, M., Reinecker, J., and Müller, B.** 2008, Borehole Breakout and Drilling-Induced Fracture Analysis from Image Logs, World Stress Map Project.

**Van Dam, D.B. and De Patter, C.J. Romijn, R**. 1999, Analysis of Hydraulic Fracture Closure in Laboratory Experiments, SPE/ISRM Eurock'98. Trondheim, Norway.

**Villarroel, F.M.G.** 2009, Physical Simulation of Wellbore Mechanical Behavior, M.Sc. Thesis, in preparation, Rio de Janeiro, Brazil.

**Zoback, M.D., Moos, D., Mastin, L., and Anderson, R.N.** 1985, Wellbore Breakouts and In-Situ Stress, Journal of Geophysical Research, Vol. 90, pp 5523-5530.

**Zoback, M.D.,** 2007, Reservoir Geomechanics, Cambridge University Press, New York, USA.

**Zoback, M.D.** 2009, Reservoir Geomechanics, GMI/Baker Hughes presentation in Rio de Janeiro, Brazil.